Mineralogy and Petrology (2018) 112 (Suppl 1):S43–S56
https://doi.org/10.1007/s00710-018-0595-6

ORIGINAL PAPER

Eclogites and garnet pyroxenites from Kimberley, Kaapvaal craton, South Africa: their diverse origins and complex metasomatic signatures

Qiao Shu[1,2] · Gerhard P. Brey[3] · D. Graham Pearson[2]

Received: 10 December 2017 / Accepted: 18 May 2018 / Published online: 5 June 2018

Abstract

We describe the petrography and mineral chemistry of sixteen eclogite and garnet pyroxenite xenoliths from the reworked Boshof road dump (Kimberley) and define three groups that stem from different depths. Group A, the shallowest derived, has low HREE (heavy rare earth element) abundances, flat middle to heavy REE patterns and high Mg# [= 100·Mg/(Mg + Fe)]. Their protoliths probably were higher pressure cumulates (~ 0.7 GPa) of mainly clinopyroxene (cpx) and subordinate orthopyroxene (opx) and olivine (ol). Group B1 xenoliths, derived from the graphite/diamond boundary and below show similarities to present-day N-MORB that were modified by partial melting (higher Mg# and positively inclined MREE (middle REE) and HREE (heavy REE) patterns of calculated bulk rocks). Group B2 samples from greatest depth are unique amongst eclogites reported so far worldwide. The calculated bulk rocks have humped REE patterns with very low La and Lu and prominent maxima at Sm or Eu and anomalously high Na_2O (up to 5 wt%) which makes protolith identification difficult. The complex trace element signatures of the full spectrum of Kimberley eclogites belie a multi-stage history of melt depletion and metasomatism with the introduction of new phases especially of phlogopite (phlog). Phlogopite appears to be characteristic for Kimberley eclogites and garnet peridotites. Modelling the metasomatic overprint indicates that groups A and B1 were overprinted by volatile- and potassium-rich melts probably by a process of chromatographic fractionation. Using constraints from other metasomatized Kimberley mantle rocks suggest that much of the metasomatic phlogopite in the eclogites formed during an intense episode of metasomatism that affected the mantle beneath this region 1.1 Gyr ago.

Keywords Eclogites and garnet pyroxenites · Cumulates · Melting of eclogite · Metasomatism

Introduction

Mafic rocks are brought to Earth's surface as eclogitic and garnet pyroxenitic xenoliths by kimberlites. Although volumetrically small they are an important and integral part of the continental lithosphere (Schulze 1989). They are derived from a wide depth range from the lower crust to the base of the lithosphere. Their protoliths were partial melts of the mantle and cumulates thereof with a history of low-pressure magmatic processes and seafloor alteration followed by subduction, dehydration, and metamorphism, metasomatism and melt loss at high pressures (summaries by Jacob 2004; Aulbach and Jacob 2016). These multiple processes will remould the original chemical and isotopic compositions and may also lead to changes in mineral assemblage. However, some diagnostic minerals such as kyanite, corundum and coesite may crystallize and some geochemical features be preserved such as Eu anomalies and $\delta^{18}O$ ratios. These characteristics allow us to deduce the protoliths to these xenoliths (e.g. Jacob et al. 1994; Smyth and Hatton 1977; Jacob 2004; Dongrea et al. 2015; Shu et al. 2016; Sommer et al. 2017).

Jacob et al. (2009) took low oxygen isotope values, overall high trace element abundances and a range of Mg# from 59.5

Editorial handling: D. B. Snyder

Electronic supplementary material The online version of this article (https://doi.org/10.1007/s00710-018-0595-6) contains supplementary material, which is available to authorized users.

✉ Qiao Shu
shuqiao@mail.gyig.ac.cn

[1] State Key Laboratory of Ore Deposit Geochemistry, Institute of Geochemistry, Chinese Academy of Sciences, Guiyang 550081, China

[2] Department of Earth and Atmospheric Sciences, University of Alberta, 126 ESB, Edmonton, AB T6G 2E3, Canada

[3] Institut für Geowissenschaften, Mineralogie, Goethe-Universität Frankfurt, Altenhöferallee 1, D-60438 Frankfurt, Germany

to 88.4 in reconstructed bulk rock compositions of eclogites from Kimberley as indicators that the protoliths were seawater-altered oceanic cumulates. We collected a new and more diverse suite of eclogites from the Boshof road dump in Kimberley that demands a more complex overall history. The greater diversity should enable us to reconstruct the origin of the Kimberley eclogites in more detail.

Samples and analyses

Petrography and samples

Eclogites from the Kimberley pipes are very scarce and have only been reported on previously by Jacob et al. (2009). The recent reworking of the Boshof Road dump -representing material derived from the Bultfontein mine - provided an opportunity to collect new samples. We recovered 16 eclogite and garnet pyroxenite xenoliths with longest dimensions of 3–6 cm from the heavy mineral concentrate of the diamond recovery plant at the former DeBeers mine in Kimberley. We studied them in hand specimen and polished probe mounts in reflected light (Fig. 1). Photographs of all samples are given in the electronic supplementary material (Fig. S1) together with the texture and modal amounts and colors of garnet (grt), clinopyroxene and orthopyroxene. The modes, estimated from the photographs by point-counting with a 1.5 · 1.5 mm grid, of grt and cpx vary between 40 and 60 vol% and 60 to 40 vol% respectively. A few samples are layered but most appear equigranular with triple junctions between grt and cpx (Fig. 1d). Depending on the composition, the xenoliths consist of orange to brown garnets and pale to dark and black green clinopyroxenes as the main constituent phases. Two samples contain opx at 3 vol% and 20 vol%. Jacob et al. (2009) also describe two opx- and one olivine-(ol) bearing sample. Half the xenoliths have minor phlog (estimated around 1 vol%) with sizes from 0.5 to 4 mm. They appear to be in textural equilibrium with the other eclogite phases as shown by triple junctions with grt and cpx (Fig. 1e) or cpx and sulfide (Fig. 1b and c). We did not observe the two generations of larger phlogopites documented by Jacob et al. (2009), one of which grew at the expense of grt and cpx. We can confirm the occurrence of secondary fine-grained phlog along grain boundaries that probably precipitated from the percolating kimberlite host magma. One sample (KimPo 8) contains minor corundum and Jacob et al. (2009) describe one kyanite bearing sample. Ilmenite (ilm; Fig. 1a) and sulfides occur in a number of samples, the latter either interstitial between phlog and cpx (Fig. 1b and c) or included in phlog (Fig. 1d). No magnetite or rutile was found in our polished mounts but a Ti-phase must be present in all samples because of strong negative Ti and Zr-Hf anomalies in their silicate trace element spectra (see below).

Analytical techniques

The silicate phases and ilmenite were analyzed for major and trace elements, and corundum was analyzed for major elements only, using electron probe micro-analyzer (EPMA) and laser ablation-inductively coupled plasma-mass spectrometry (LA-ICP-MS) analysis. Major elements were measured by EPMA in the wave-length-dispersive mode (WDS) with a JEOL JXA 8900RL. Each sample was mounted in epoxy and polished. Five to six spots were analyzed on each grain to test for compositional homogeneity. The acceleration potential was 15 kV, the beam current 20 nA and the spot size 3 μm. Counting times varied between 40 and 20 s on peak and background. All elements were measured by their Kα-lines on natural and synthetic standards. Sodium was measured at the beginning of the measuring sequence for 20 s each on peak and on one background with albite as a reference material and a TAP crystal. Olivine was used as calibrant material for Mg (TAP), $KTiPO_5$ for K and P (PET), Cr_2O_3 for Cr (PET), Al_2O_3 for Al (TAP), $CaSiO_3$ for Ca (PET) and Si (TAP), $MnTiO_3$ for Ti (PET), MnO for Mn (LIFH), Fe_2SiO_4 for Fe (LIFH) and NiO for Ni (LIFH). Mn, Fe and Ni were measured on a H-type spectrometer (Rowland circle $R = 100$ mm). Data reduction was carried out with the CITZAF correction program (version 3.5) for quantitative electron microbeam X-ray analysis (Armstrong 1991, 1995). The full data set is given in the electronic supplementary material (Tables S1-S3).

Trace-element analyses on grt and cpx were carried out on a Thermo Element 2XR ICP-MS linked to a 193 nm M-50 HR Laser (Resonetics), using the reference glass NIST 612 as a calibration standard for minerals (garnet and cpx) and natural basalt glass reference material BIR-1 glass to monitor instrument performance. The Iolite program was employed for data reduction.

Trace element analyses on phlogopites and ilm were conducted by LA-ICP-MS with a GeoLas 2005 laser coupled to an Agilent 7500a quadrupole ICP-MS. Operating conditions for the laser ablation system and the ICP-MS instrument and data reduction are described by Liu et al. (2008) in detail. Each analysis incorporated a background acquisition of approximately 20 s (gas blank) followed by 50 s data acquisition from the sample. Element contents were calibrated against multiple-reference materials (BCR-2G, BIR-1G and BHVO-2G) without applying internal standardization (Liu et al. 2008). The preferred values of element concentrations for the USGS reference glasses are from the GeoReM database (http://georem.mpch-mainz.gwdg.de/; Jochum et al. 2005). Off-line selection and integration of background and analyte signals, and time-drift correction and quantitative calibration were performed by ICPMSDataCal (Liu et al. 2008, 2010). The averaged data are shown in the electronic supplementary material (Tables S4-S5). The full set of analyses and a statistical evaluation (average instrumental uncertainty, standard

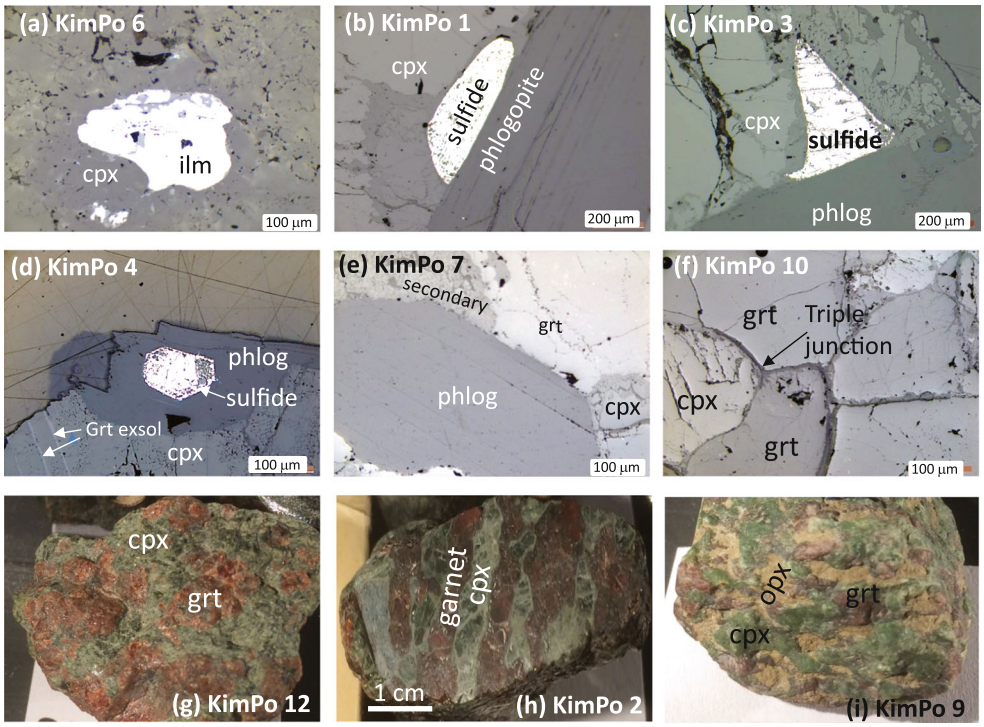

Fig. 1 Reflected light pictures of polished mounts and photographs of selected hand specimens: **a** ilmenite inclusion in cpx **b** sulphide between phlogopite and clinopyroxene **c** sulphide interstitial between clinopyroxene and phlogopite. **d** phlogopite with a sulfide inclusion next to clinopyroxene with thin garnet exsolution lamellae **e** phlogopite with triple junction with garnet and clinopyroxene as equlibrium texture **f** triple junction between garnet and clinopyroxene grains **g** Kimpo 12 (Group B1) with equigranular texture **h** KimPo 2 (Group B2) with layering of garnet and clinopyroxene **i** KimPo 9 (Group A-opx) with equigranular texture of garnet, clinopyroxene and orthopyroxene

deviations for multiple analyses per sample) are shown in supplementary material Table S6.

Results

Mineral compositions

Major element chemistry and sample classification

Averaged major element compositions of the primary phases grt, cpx, opx and phlog are provided in Tables S1-S3. Garnets and clinopyroxenes are homogeneous within analytical errors. Garnets were divided into groups A (with A-opx), B1 and B2 in the classification scheme of Coleman et al. (1965) (Fig. 2a). The distinction between groups B1 and B2 was made on the basis of the higher Na-contents in Group B2 clinopyroxenes. These plot at the boundary of and into the Group C field of Taylor and Neal (1989). The grt and cpx compositions of Jacob et al. (2009) plot with our A and B1 groups (A and B after Taylor and Neal 1989). One garnet from the kyanite bearing sample of Jacob et al. (2009) contains the highest grossular content but the coexisting cpx plots in Group B1. We use the Group A (A-opx), B1 and B2 classification in all following diagrams and tables.

Group A xenoliths contain pyrope-rich garnets (mostly around Py70Alm10Grs20) associated with jadeite-poor clinopyroxenes (up to 3 wt% Na_2O; Fig. 2b) and are therefore garnet pyroxenites. Group B1 xenoliths have garnets ranging from $Py_{48}Alm_{34}Grs_{18}$ to $Py_{57}Alm_{25}Grs_{18}$ and omphacites with 3–5 wt% Na_2O, 10–14 wt% MgO (Fig. 2b) and 10–14 wt% CaO. Group B2 xenoliths are eclogites sensu stricto. They possess more Ca-rich garnets ranging from $Py_{35}Alm_{34}Grs_{31}$to $Py_{52}Alm_{28}Grs_{20}$ associated with jadeite-rich (45–58 mol%) clinopyroxenes (6.5 to almost 9 wt% Na_2O) with low Mg#. Including the data of Jacob et al. (2009) there is a tendency of increasing Cr_2O_3 with Mg# in cpx from Group B1 to A (Fig. 2c). The Cr_2O_3 contents range from 0.1 to 1.5 wt%. Orthopyroxene has always much lower Cr_2O_3 contents than coexisting cpx.

At least half of the xenoliths presented here and of Jacob et al. (2009) contain phlogopite. Phlogopite Mg# correlate positively with those of coexisting garnet whereby Mg# of phlog is always higher than Mg# of garnet (Fig. 2d). The Mg# of phlog also correlates positively with that of cpx though with more scatter. The grouping established by the grt and cpx compositions is also reflected in the phlog compositions.

Trace element chemistry

Trace element data of garnet and cpx are provided Table S6. Amongst our Group A garnet pyroxenites, the garnets from the two opx-bearing varieties and another A sample have flat to slightly positive inclined middle to heavy REE at about ten times chondrite abundances and elevated LREE (Fig. 3a). Two further Group A garnets have slightly to strongly positive inclined middle to heavy REE and depleted LREE. Group B1 garnets also have strongly positive sloped middle to heavy

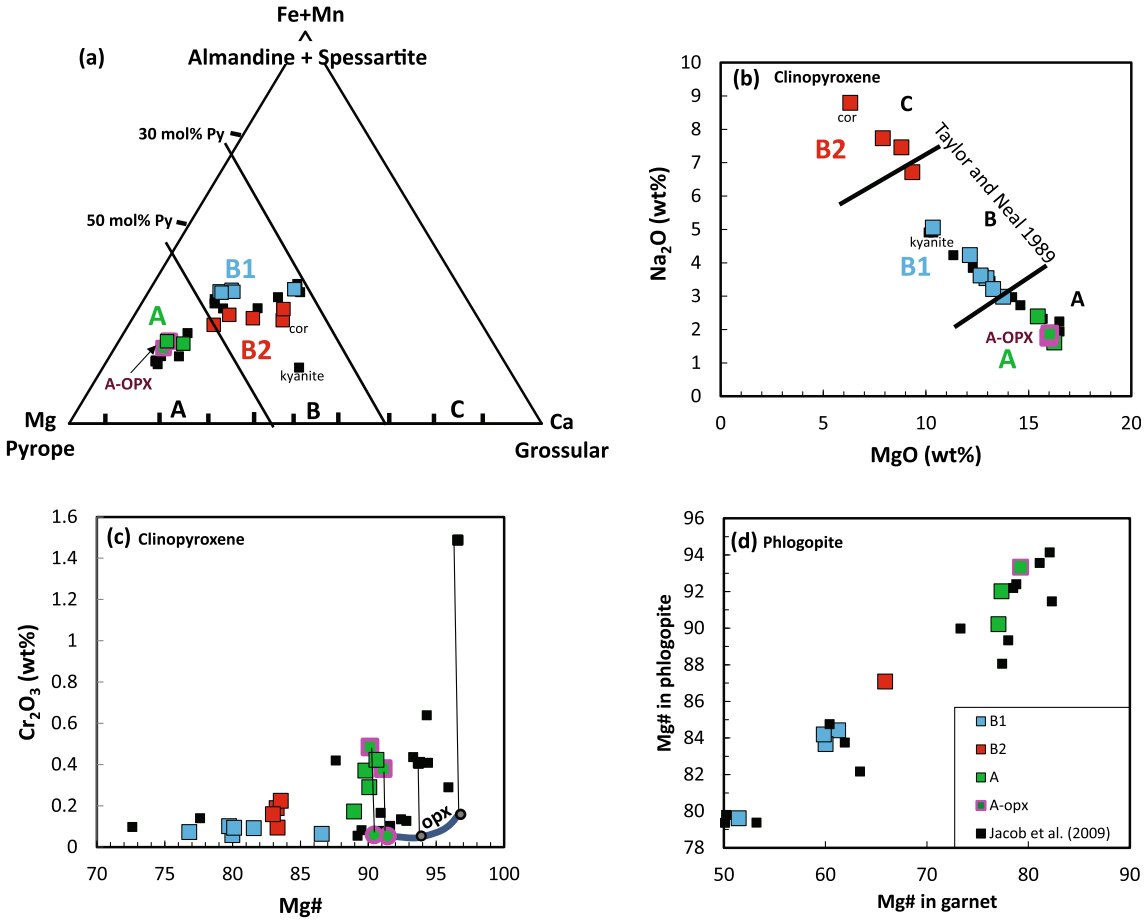

Fig. 2 Major element compositions of garnets and clinopyroxenes **a** Garnet triangular diagram after Coleman et al. (1965) with their eclogite nomenclature scheme with own data and Kimberley eclogite data from Jacob et al. 2009. All Kimberley eclogites plot into the A and B fields. We subdivided samples in B into B1 and B2 by criteria from the compositions of clinopyroxenes and REE patterns **b** Diagram of MgO versus Na_2O showing the compositional range of clinopyroxenes: the division A, B and C of Taylor and Neal (1989) is also shown by dashed black lines. Our group B2 sampled plot into the group C field of Taylor and Neal 1989 **c** Diagram of Mg# versus Cr_2O_3 of clinopyroxenes and orthopyroxenes from Kimberley eclogites; coexisting opx and cpx are connected by the dashed lines **d** Plot of Mg# of phlogopite versus Mg# of garnet: there is a positive correlation slope with highest Mg# in Group A samples and lowest in Group B1

REE but at much higher concentrations than A. Their LREE are also depleted with an upward kick at La and Ce. Group B2 patterns are unique amongst eclogitic garnets reported so far with negatively sloped middle to heavy REE (HREE) and extremely strong fractionated and positively sloped LREE with very low abundances leading up to a hump in the MREE.

Clinopyroxenes of all Groups have steeply inclined REE patterns with low to very low HREE and LREE peaks at Ce (Fig. 3c). Such steep REE patterns in cpx correspond to the equilibration with coexisting garnet (Fig. S2). Garnet and cpx REE partition coefficients can be a function of pressure or temperature (e.g. Klemme et al. 2002). Accordingly, our Group B2 samples with the highest equilibration temperatures have the highest partition coefficients ($D^{grt/cpx}$) while Group A xenoliths with the lowest temperatures yield lowest D values. Partition coefficients can also depend strongly on the major element composition, especially Na in cpx and Ca in grt (e.g. Harte and Kirkley 1997). Accordingly, $D^{grt/cpx}$ are highest for Group B2, intermediate for B1 and lowest for A samples, i.e. they are positively correlated with Na_2O in cpx.

Both garnets and clinopyroxenes have strong, negative Ti, Zr-Hf and Nb-Ta anomalies (Fig. 3b and d) in all sample types. These are in all likelihood due to coexisting rutile or ilm as described by Jacob et al. (2009) in their samples. We found only one ilmenite in a polished mount; otherwise these phases were not visible in hand specimen nor in our polished probe mounts.

The trace element pattern of the single ilm observed in our samples is shown in Fig. 4a and given in the electronic supplementary material (Table S4). It has a similar trace element pattern similar to those measured by Jacob et al. (2009) in their Kimberley samples. The Nb-Ta contents lower than Nb-Ta concentrations in two ilmenites from a Bultfontein peridotite (Konzett et al. 2000) but the Nb/Ta ratios are similar between 13 to 23. The abundances of Cr, Mn, Co, Ni and Zn are similar in eclogites and peridotites.

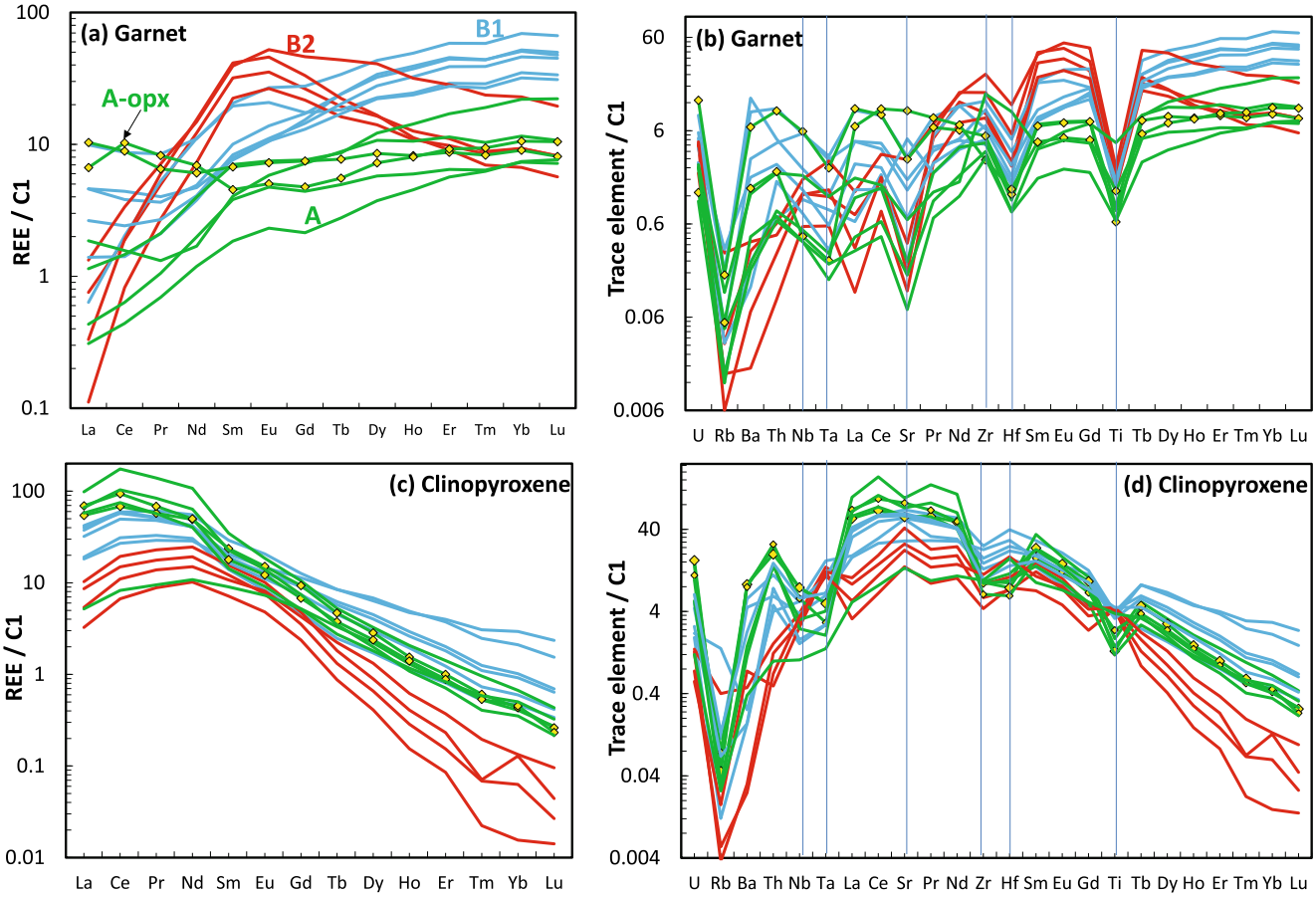

Fig. 3 Chondrite-normalized REE and trace element diagrams for garnets and clinopyroxenes. Chondrite composition is taken from Sun and McDonough (1989). Consistent with major elements, three groups are apparent: A (A-opx), B1 and B2. **a** grt REE patterns **b** grt trace element patterns **c** cpx REE patterns **d** cpx trace element patterns

The averages of 3 to 5 analyses per grain on phlogopites from 6 samples (1 to 4 grains depending on sample) are given in the electronic supplementary material (Table S5) and shown in Fig. 4b together with the data from Jacob et al. (2009) and phlogopites from the same peridotite sample as the ilm above (Konzett et al. 2000). The phlogopites from our study are homogenous within grains and from grain to grain. All samples display similar features, such as high Ba contents, positive Nb-Ta, Sr and Ti anomalies but no Zr-Hf anomalies. The samples from Jacob et al. (2009) are very similar except that four of them also have positive Zr-Hf anomalies. The phlogopites from the peridotite sample also have positive Zr-Hf anomalies but no Sr anomaly. The Nb-Ta anomalies are lower in the peridotitic than in the eclogitic phlogopites. The

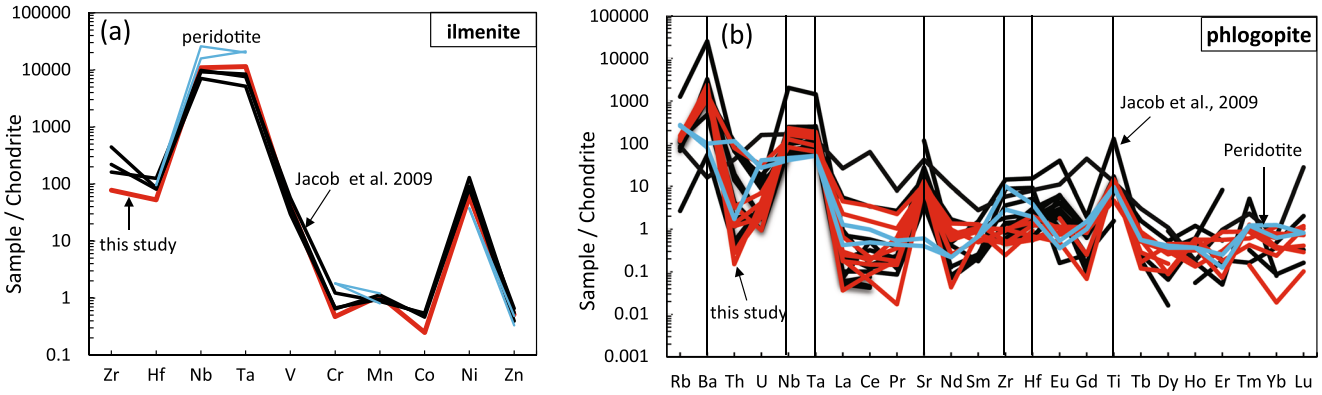

Fig. 4 Chondrite-normalized trace element diagrams for **a** ilmenite and **b** phlogpite from this study (red patterns) and from a previous study (black patterns) on Kimberley eclogites by Jacob et al. (2009) and for comparison from a Bultfontein peridotite (light-blue patterns; Konzett et al. 2000). Chondrite composition is taken from Sun and McDonough (1989)

Nb/Ta ratios range from 21 to 25 in our samples and from 7 to 25 in the samples of Jacob et al. (2009). The phlogopites have overall low REE contents and relatively high HFSE and Ti contents. Relative to the REE the latter elements partition more strongly into phlog than grt or cpx (Fig. S3 in the electronic supplementary material). The partitioning for Zr and Hf is similar with both phases irrespective whether the Zr-Hf anomalies in phlog are high or low. We take this and the regular patterns of the partition coefficients as indication of equilibrium between the three phases.

Reconstructed bulk rock compositions

Note that this chapter incorporates a data set of Jacob et al. (2009). Because of generally small sizes and a likely contamination by the host kimberlite magma, whole rock compositions of mantle xenoliths are often reconstructed from mineral compositions and their modal abundances (e.g. Barth et al. 2001; Jacob et al. 2005). Modal abundances for Kimberley eclogites were obtained by Jacob et al. (2009) by point-counting of thin sections. They determined modal garnets as 70 to 30 vol%, for cpx between 30 to 70 vol% and for phlog up to 10 vol%. They found opx in two samples and rutile, kyanite and olivine in one sample each. We have point-counted grt, cpx and opx in the photographs of our hand specimens (electronic supplementary material Fig. S1) but did not include phlog because of the small modal amounts. Neglecting phlog mainly results in too low K, Rb, Ba Ti and HFSE in calculated bulk rocks. The calculated bulk trace element data are given in Table 1. The REE abundances are practically unaffected due to very low REE in phlog (Fig. 4b). Errors from point-counting small samples may be fairly large. However, since the grain sizes range to a maximum of about 5 mm in our samples and because the phases are generally evenly distributed, the results of point-counting our samples should be representative. We visualize the effect of an absolute error of ±10 vol% on the amount of garnet obtained by point-counting in Fig. 5 as error bars on the symbols for our samples. The clear distinction between the various eclogite types and the composition of mid-ocean ridge basalts (MORB) remains. We have also estimated the metamorphic mineral modal abundances for the average of Indian Ocean N-MORB glasses [see Table 1.2.5.2 in Basaltic Volcanism Study Project 1981] with the program Theriak/Domino (de Capitani and Petrakakis 2010). The mode calculations for equilibrium at 1150 °C and 40 kb give a high-pressure mineral assembly of 43.2 vol% grt, 54.3 vol% cpx, 2.2 vol% ilm and 0.2 vol% rutile. The modal amounts of grt and cpx are close to those we estimated by point counting of hand specimens for group B1 samples. Such calculations are difficult for Group A and B2 samples because of a more uncertain choice for a precursor rock (protolith). Because of this difficulty, we use the modal abundances from point counting for all groups to calculate bulk rock compositions.

We have evaluated the effect of varying grt:cpx ratios on the REE patterns of calculated whole rock compositions (electronic supplementary material Fig. S4) and find that they are relatively robust to large changes in modal amounts of garnet and cpx (see also Jerde et al. 1993). The calculated bulk major element compositions are given in Table 1 and the relationships between some elements and Mg# shown in Fig. 5a–c. along with data from Jacob et al. (2009), MORB and picrite compositions, a compositional field for modern day troctolites and the compositions of kyanite and corundum eclogites from Bellsbank (Shu et al. 2016). Groups A and B1 overlap completely with the samples of Jacob et al. (2009) while B2 samples extend to very much higher Na_2O and Al_2O_3 contents (Fig. 5a). Group B1 eclogites overlap with the MORB field while Group A xenoliths plot along a potential trend for ol + cpx ± opx accumulation. The B2 samples have much higher Na_2O contents than modern day troctolites from the Pacific (Perk et al. 2007) while Bellsbank kyanite and corundum eclogites plot close to this field as well as one kyanite-bearing sample from Kimberley. Figure 5b serves to show that picrites and troctolites are generally too Ni rich to serve as protoliths for Kimberley eclogites respectively Group B2 eclogites and that all Kimberley samples have higher Mg# than MORB. Figure 5c again serves to illustrate the differences to MORB and to show that these may be due to cumulate processes and/or partial melting.

The results of the re-constructed bulk rock trace element concentrations for the Kimberley eclogites are shown in Fig. 6a–c (plus Supplementary Fig. S5). Almost all Group A garnet pyroxenites are strongly enriched in LREE with a hump at Ce (Fig. 6a). They have the highest LREE and the lowest HREE of all samples. Five samples have flat middle to heavy REE (5 to 7 times C1 chondrite) while three are positively inclined from Tb onwards. One sample (KimPo 17) has low LREE slightly declining towards La and one sample has a REE pattern with a hump at Sm that is similar to the REE patterns of the Group B2 samples (Fig. 6c).

The majority of the B1 eclogites have sinusoidal REE patterns with a hump at around Pr and a few at Nd. All samples except for one have positively sloped REE patterns from Tb onwards (Fig. 6b). REE abundances are variable with La_N ranging between 14 and 38. Three samples with highest modal amounts of grt have the highest Lu_N abundances of between 55 and 85 x chondrite. LREE depletion in two samples) are sub-parallel to N-MORB. The kyanite-bearing sample has the lowest REE contents with $Lu_N = 1.1$, a positive Eu-anomaly and a humped LREE pattern.

Group B2 samples have humped REE patterns (Fig. 6c) with about 35 times C1 chondrite at Sm or Eu and strong depletion in both light and heavy REE contents, e.g. $La_N = 1.6$ and $Lu_N = 4$ for the corundum bearing sample KimPo 8.

Table 1 Major and trace element compositions of reconstructed bulk rocks of Kimberley eclogites

Group	B2	B2	B2	B2	B1	B1	B1	B1	B1	B1	A	A	A	A	A	A
Sample	KimPo2	KimPo7	KimPo8	KimPo14	KimPo1	KimPo3	KimPo4	KimPo6	KimPo12	KimPo15	KimPo9	KimPo10	KimPo5	KimPo11	KimPo13	KimPo17
Grt:cpx modal abundances (vol%)	45:55	55:45	45:55	60:40	50:50	50:50	45:55	60:40	50:50	50:50	35:45	39:58	40:60	55:45	40:60	50:50
Further phases		phlog (1 vol%)	corundum		phlog (<1 vol%)	phlog	phlog (1 vol%)	phlog (1 vol%)			opx (20 vol%)	phlog (1 vol%), opx (3 vol%)		phlog (<1 vol%)		
Major oxides (wt%):																
SiO_2	48.55	46.97	48.43	45.70	47.89	46.65	48.48	45.65	47.48	47.75	50.41	49.95	50.05	47.13	49.62	48.13
Na_2O	4.28	3.06	4.87	3.04	1.79	2.56	2.35	1.53	1.63	1.52	0.81	1.09	1.15	0.74	1.11	1.23
CaO	10.86	10.39	11.09	11.65	11.98	13.98	12.38	11.47	12.41	13.24	10.99	13.74	14.05	11.99	13.91	12.27
MnO	0.14	0.19	0.13	0.28	0.34	0.27	0.45	0.35	0.28	0.23	0.21	0.19	0.20	0.30	0.21	0.25
MgO	10.27	12.22	8.61	10.12	13.59	9.99	12.75	13.10	13.75	14.90	20.96	18.21	17.56	18.12	17.55	17.15
Cr_2O_3	0.08	0.18	0.16	0.15	0.06	0.06	0.10	0.09	0.09	0.08	0.46	0.41	0.36	0.53	0.33	0.23
FeO^{total}	7.37	8.88	6.92	9.50	10.92	10.89	10.24	11.85	10.73	8.03	6.29	5.46	6.17	6.99	6.01	6.71
Al_2O_3	17.91	17.68	19.42	19.22	13.68	15.17	13.47	15.49	13.49	13.97	9.30	10.64	10.93	13.76	10.84	13.36
TiO2	0.21	0.19	0.25	0.21	0.18	0.26	0.24	0.22	0.19	0.23	0.08	0.13	0.11	0.06	0.09	0.32
Total	99.67	99.75	99.88	99.87	100.43	99.84	100.46	99.75	100.05	99.96	99.51	99.83	100.57	99.62	99.67	99.66
Mg#	71	71	69	66	69	62	69	66	70	77	86	86	84	82	84	82
Trace elements (ppm):																
U	0.020	0.013	0.017	0.023	0.026	0.018	0.047	0.041	0.024	0.034	0.111	0.050	0.014	0.054	0.043	0.027
Rb	0.810	0.022	0.029	0.048	0.067	1.650	0.335	0.301	0.448	0.192	0.234	0.152	0.157	0.104	0.051	0.050
Ba	1.050	0.057	1.070	0.469	3.810	0.592	17.900	23.801	2.490	2.850	18.500	12.100	1.970	8.450	1.881	2.061
Th	0.032	0.018	0.012	0.019	0.133	0.068	0.313	0.156	0.149	0.250	0.445	0.447	0.045	0.289	0.198	0.268
Nb	0.638	0.390	0.476	0.589	0.866	0.766	1.292	0.699	0.384	0.792	1.671	0.808	0.362	0.808	0.395	0.393
Ta	0.111	0.079	0.100	0.083	0.039	0.118	0.098	0.044	0.023	0.048	0.052	0.023	0.018	0.031	0.026	0.018
La	1.200	1.110	0.460	0.699	4.340	2.340	5.961	2.380	5.040	5.161	8.200	9.761	0.836	9.451	6.190	9.431
Ce	5.5	5.6	2.8	3.9	16.6	10.1	22.3	8.0	18.3	18.7	25.4	34.5	3.0	43.3	20.8	38.2
Sr	107	136	56	77	205	193	286	90	215	245	236	366	51	281	190	319
Pr	1.110	1.090	0.700	0.909	2.411	1.770	3.451	1.280	2.500	2.510	3.214	3.840	0.502	5.300	2.410	4.711
Nd	7.3	6.9	5.7	6.8	10.4	9.5	16.2	6.6	10.5	10.1	13.6	14.0	2.9	20.7	8.6	17.8
Zr	28.3	32.0	35.5	72.5	42.1	37.1	74.1	57.7	42.4	28.0	28.1	18.6	46.7	24.4	21.4	26.6
Hf	0.540	0.626	0.698	1.471	1.360	0.998	2.470	1.430	1.261	0.831	0.499	0.418	1.400	0.435	0.485	0.746
Sm	3.1	2.9	3.3	4.1	2.1	2.5	3.7	2.0	2.0	1.8	2.4	1.8	1.0	2.7	1.1	2.2
Eu	1.1	1.1	1.3	2.0	0.7	0.8	1.3	0.8	0.7	0.6	0.7	0.5	0.4	0.7	0.3	0.6
Gd	2.7	2.8	3.2	5.9	2.7	2.2	3.9	2.8	2.3	2.0	1.7	1.2	1.2	1.7	0.7	1.2
Ti	1260	1170	1430	1430	1040	1390	1320	1210	1060	1370	444	841	1810	569	394	542

Table 1 (continued)

Group	B2	B2	B2	B2	B1	B1	B1	B1	B1	B1	A	A	A	A	A	A
Sample	KimPo2	KimPo7	KimPo8	KimPo14	KimPo1	KimPo3	KimPo4	KimPo6	KimPo12	KimPo15	KimPo9	KimPo10	KimPo5	KimPo11	KimPo13	KimPo17
Grt:cpx modal abundances (vol%)	45:55	55:45	45:55	60:40	50:50	50:50	45:55	60:40	50:50	50:50	35:45	39:58	40:60	55:45	40:60	50:50
Further phases		phlog (1 vol%)	corundum		phlog (<1 vol%)	phlog	phlog (1 vol%)	phlog (1 vol%)			opx (20 vol%)	phlog (1 vol%), opx (3 vol%)		phlog (<1 vol%)		
Tb	0.341	0.351	0.380	0.979	0.589	0.375	0.720	0.610	0.469	0.389	0.219	0.165	0.219	0.262	0.100	0.147
Dy	1.900	2.000	1.900	6.150	5.020	2.990	5.650	5.210	3.910	3.100	1.330	1.120	1.590	2.120	0.706	0.861
Ho	0.318	0.337	0.281	1.050	1.200	0.700	1.350	1.290	0.961	0.700	0.248	0.239	0.325	0.512	0.165	0.166
Er	0.811	0.880	0.661	2.750	3.940	2.390	4.560	4.390	3.250	2.300	0.716	0.740	0.978	1.730	0.557	0.481
Tm	0.099	0.116	0.078	0.353	0.574	0.362	0.689	0.660	0.495	0.340	0.100	0.112	0.134	0.292	0.092	0.069
Yb	0.681	0.834	0.487	2.220	4.260	2.850	5.280	5.090	3.790	2.620	0.692	0.807	0.963	2.170	0.694	0.506
Lu	0.091	0.111	0.063	0.289	0.605	0.418	0.771	0.743	0.561	0.386	0.093	0.119	0.136	0.332	0.107	0.074

Such REE patterns are unique for mantle eclogites but a similarly shaped pattern with higher La and Lu abundances and a lower hump exists amongst the Group A samples (Fig. 6a).

Nearly all samples show pronounced negative Ti- and HFSE anomalies, also shown in those samples where Jacob et al. (2009) included phlogopite and rutile in the bulk rock calculations (electronic supplementary material Fig. S5). Assuming that there were no anomalies in the protolith and using the Ti anomaly as a measure as suggested by Aulbach and Viljoen (2015), we calculate an amount of 0.04 to 0.5 vol% rutile that should be present in the rocks.

Geothermobarometry

Temperatures of last equilibration were calculated with the grt-cpx Fe^{2+}-Mg^{2+} exchange thermometer of Krogh (1988) (electronic supplementary material Table S7). We used the averages of EPMA analyses of grt and cpx and did not correct for the possible presence of Fe^{3+} in these phases. The calculation of Fe^{3+} from structural formula would be quite inaccurate since the sums of cations are close to 8 respectively 4 anyway indicating very low Fe^{3+}. Also, Purwin et al. (2012) found high pressure experiments at varying oxygen fugacities that temperature estimates with Krogh (1988) reproduce experimental temperatures to ±60 °C if total Fe is used. The derived temperatures were projected in iterative steps onto geothermal gradient for lithospheric mantle underneath the Kimberley mine as derived by Mather et al. (2011). The three groups mainly fall into three pressure-temperature ranges: Group A samples lie between 930 to 970 °C and 3.9 to 4.1 GPa, Group B1 samples between 1038 to 1110 °C and 4.6 to 5.1 GPa and Group B2 yields the highest temperatures and pressures from 1175 to 1236 °C and 5.6 to 6.2 GPa. The P-T conditions of the samples described by Jacob et al. (2009) lie within the range of B1.

Discussion

Protoliths – evidence from major and trace elements

Despite the probable loss of a melt fraction from this suite of eclogites and severe overprint by metasomatism, some vestigial features in the major elements and less incompatible (middle to heavy REE) and compatible (Ni, Cr) trace elements remain diagnostic of their protoliths.

Group A garnet pyroxenites plot at low Al_2O_3 and Na_2O and have the highest Ni and Mg# of all groups (Fig. 5a and b). They also have the highest SiO_2 (CaO and MgO) contents but their compositions do not coincide with MORB or picrites (Fig. 5a–c). Residua of eclogite melting would have high CaO and MgO but SiO_2 would be lowered. Also, middle to heavy REE are compatible in garnet and therefore would

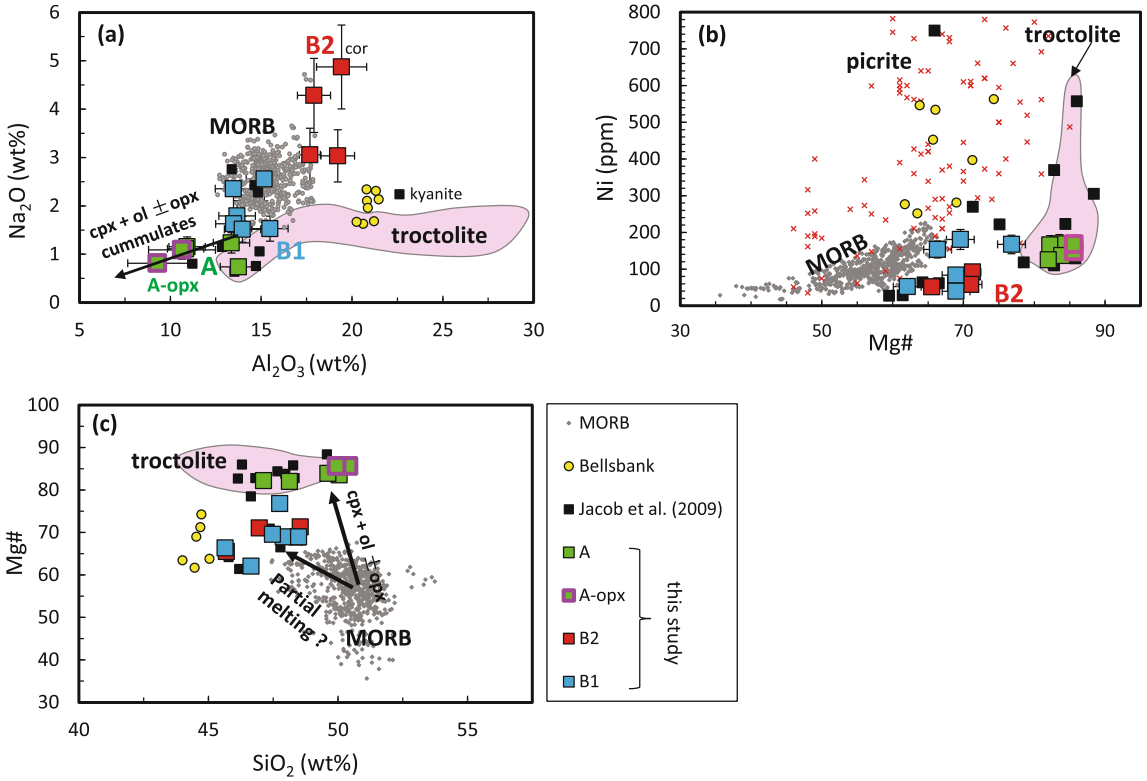

Fig. 5 Reconstructed bulk rock compositions of eclogite from this study are shown in comparison with the Kimberley eclogite data from Jacob et al. (2009), Bellsbank eclogite data from Shu et al. (2016), with MORB and picrite compositions and a field for troctolites Perk et al. (2007): **a** Al_2O_3 vs. Na_2O of calculated bulk rock compositions. Only group B1 samples overlap with MORB (data from Jenner and O'Neill 2012). Group B2 samples have the highest Al_2O_3 and Na_2O contents while group A samples the lowest Al_2O_3 and Na_2O contents. The latter are interpreted as pyroxene dominated ol (opx) + cpx cumulates as indicated by the black arrow. **b** Concentrations of Ni vs. Mg# compared with MORB and intraplate and Archean cratonic picrites from GEOROC (http://georoc.mpch-mainz.gwdg.de). **c** Mg# vs. SiO_2 for calculated bulk rock compositions. The vast majority of eclogites have lower SiO_2 and higher Mg# compared to modern MORB samples. Group B1 samples with higher Mg# and lower SiO_2 than MORB can be interpreted as residues of partial melting in the eclogite stability field. Protoliths for Group A samples with higher SiO_2 contents and Mg# were probably cpx-rich cumulates

increase in the residue. However, Group A garnet pyroxenites have the lowest HREE contents. They also have the highest Cr_2O_3 contents in their clinopyroxenes (Fig. 2c). All these features point to a cumulate origin with mainly cpx (and possibly some ol/opx) as an accumulating phase. Plagioclase was not among the accumulating phases because of the absence of a Eu-anomaly. Therefore, phase accumulation must have occurred at somewhat elevated pressures of around 0.7 GPa as required by the liquidus phase relationships of mafic magmas (Green and Ringwood 1967; Presnall et al. 1978) requiring a thicker oceanic crust than today. A cumulate origin for the protoliths of the Kimberley eclogites with similar compositions was also suggested by Jacob et al. (2009) and a similar origin for other eclogites also invoked by Barth et al. (2001) and Schmickler et al. (2004).

Group B1 samples have compositions roughly intermediate between Group A (high-Mg samples) and Group B2 (high-Al samples) and plot within or in the vicinity of the MORB samples in the Na_2O vs. Al_2O_3 diagram. But they have remarkedly higher Mg# and slightly higher CaO and lower SiO_2 contents compared to MORB samples and coincide with Group B2 in Mg# and SiO_2. (Fig. 5a–c). Higher Mg# and lower SiO_2 than MORB are the characteristic features of the residues from partial melting of such compositions in the eclogite stability field. Combined with evidence from middle to heavy REE abundances and their fractionated patterns our hypothesis for the modelling below is that B1 samples were formed as residues of partial melting of MORB-like eclogites and subsequently metasomatized as indicated by the LREE enriched patterns.

The Na_2O contents of the Group B2 eclogites are amongst the highest that have been reported for eclogites from the Kaapvaal craton and their Al_2O_3 contents are only surpassed by the corundum-bearing eclogites from Bellsbank (Shu et al. 2016). They plot above the MORB field in Na_2O-Al_2O_3, at higher Mg# and at lower SiO_2 (Fig. 5a–c). In principle, they could represent olivine + plagioclase cumulates (troctolites). However, they plot away from troctolites in almost every chemical aspect such as too high Na_2O and too low Mg# and Ni-contents. The total REE abundances are higher than in troctolites and correspond to gabbros (Fig. 6c) but the shape of the REE pattern does not correspond to gabbros and is

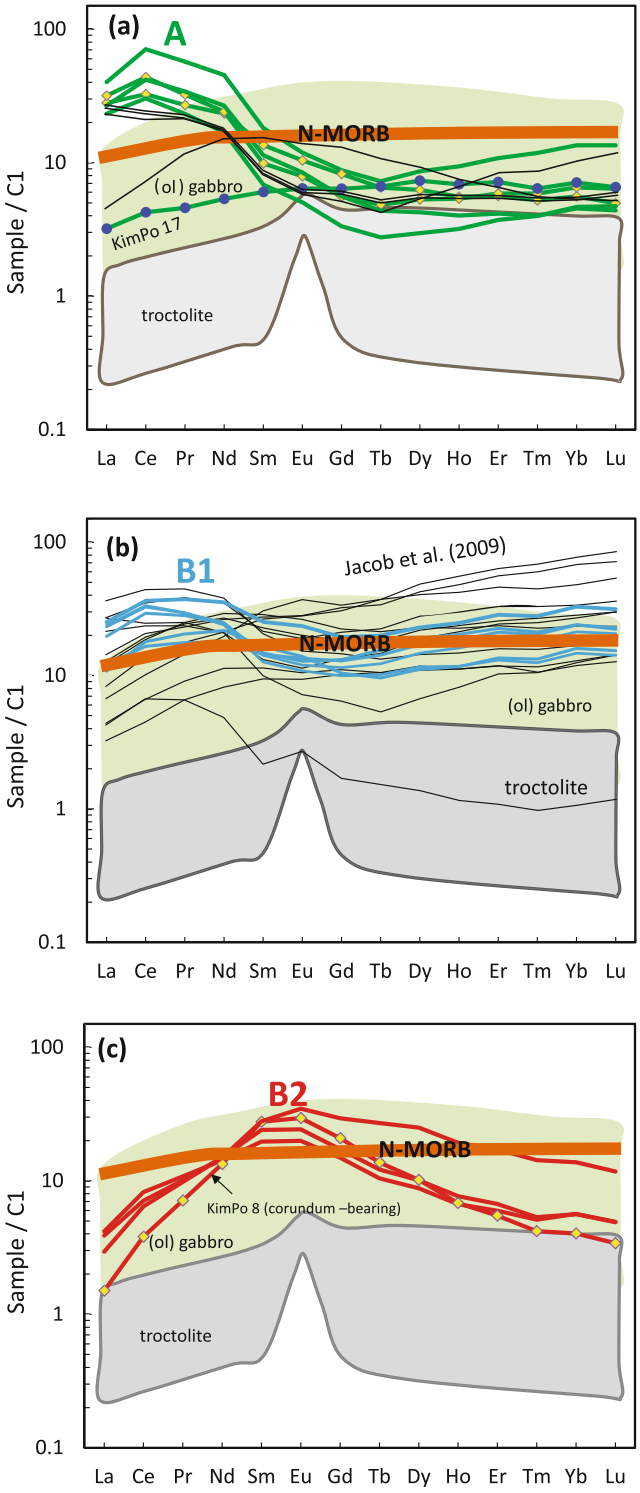

◀ **Fig. 6** Chondrite-normalized REE and trace element patterns for reconstructed bulk rock compositions (Table 1). Chondrite composition is taken from Sun and McDonough (1989). The three groups are shown separately. The average N-MORB REE composition of Sun and McDonough (1989) is shown for reference as dark yellow line in all three diagrams as well as the range of troctolite compositions from Pito Deep, Pacific ridge (Perk et al. 2007) as grey shaded field and the compositional field of (ol) gabbros from MARK region, mid- Atlantic ridge (Casey 1997) as the greenish field. The black thin lines are the patterns for the Kimberley eclogites studied by Jacob et al. (2009). **a** REE patterns of calculated bulk group A samples **b** REE patterns of calculated bulk group B1 samples **c** REE patterns of calculated bulk group B2 samples

unique for eclogites worldwide. La_N and Lu_N are very low in B2 samples and Eu_N defines the top of a pronounced hump of the REE patterns.

We were not able to pin-point potential protoliths for these unique kinds of eclogites. Possibilities include highly altered basalts, gabbros or higher pressure clinopyroxene-spinel cumulates. Sodium would have to be introduced subsequently in all cases, the Al-content increased for basalts and gabbros and the REE patterns completely changed. Sodium could be introduced to the rocks by low-temperature alteration and spilitisation on the ocean floor or by higher temperature hydrothermal alteration. Hydrothermal alteration and transportation of REE by fluoride complexes deeper in the ocean crust may change the REE patterns and abundances (Hellman and Henderson 1977; Williams-Jones 2015). It is, however, not clear in which direction this process goes. As these samples reside at the base of the lithosphere it is possible that their Na contents have been elevated by interaction with saline metasomatic fluids, such as those found in some diamonds (Weiss et al. 2015), however no diamonds have been found in these Kimberley samples.

Metasomatism and partial melting of Kimberley eclogites– evidence from incompatible trace elements

Modal metasomatism

Kimberley eclogite xenoliths appear to represent a rare eclogite population where petrologically equilibrated phlog is a very common phase. Other possible metasomatic phases are rutile and ilm (Heaman et al. 2006) and sulfides. Equilibrated phlog is evidence for modal mantle metasomatism caused by subsolidus fluid or melt infiltration at lithospheric mantle condition (e.g. Dawson and Smith 1977; Erlank et al. 1987; Simon et al. 2007). Ilmenite and rutile are present in MARID suite xenoliths as major phases and are also reported from polymict breccias (e.g. Lazarov 2008). These lithologies are ascribed to melt metasomatism and kimberlite-like melt pockets that were trapped at mantle depths and crystallized. Trace elements of the ilmenites from Kimberley eclogites (Fig. 4a) show similar features to those from metasomatic ilm in peridotite xenoliths with high abundances of high field strength elements (Zr-Hf, Nb-Ta) and also resemble ilm in MARID suite xenoliths (Waters 1987; Konzett et al. 2000). These similarities point to a metasomatic origin of ilm in the Kimberley eclogites. Rutile may be primary and exsolved from garnet and clinopyroxene during metamorphism (Ringwood 1975) or may be introduced by metasomatism (Jacob et al. 2009;

Barth et al. 2001). Jacob et al. (2009) describe modal rutile from their samples and we infer its ubiquitous presence from the Ti anomalies measured in silicates.

Because phlog (except the secondary generation of fine-grained phlog along grain boundaries) is in textural and chemical equilibrium with grt and cpx, the metasomatism responsible for its growth must be older than the kimberlite magmatism. Hopp et al. (2008) determined $^{40}Ar/^{39}Ar$ ages of phlogopites from Bultfontein garnet peridotites. They found an age cluster of 1.0 to 1.22 Ga that can be equated to the Khibaran orogenesis (Namaqua-Natal), concluding that this orogenesis caused metasomatism in the cratonic mantle at that time. In addition, Pearson (1999) showed that the Nd isotope evolution lines of diopsides in Bultfontein (Kimberley) peridotites converge at circa 1 Ga, also providing support for intense metasomatism in the Kimberley mantle at this time which likely also affected the eclogites. The time elapsed since then promote full textural equilibration. The ubiquitous metasomatic agent must have been a volatile- and K-rich melt or fluid such as a carbonatite or kimberlite melt that infiltrated the thick cratonic lithosphere and precipitated phlog and ilm.

Cryptic metasomatism and partial melting

Cryptic metasomatism may result from the same process as modal metasomatism, differing only locally in intensity. The local differences are most likely related to variations in melt-rock ratio that can be a function of the proximity to the main melt channel. Also, phase precipitation may not occur, even if melt-rock ratios are high because the P, T conditions and other parameters are not within the stability field of a mineral like phlog. The P, T conditions of the Kimberley eclogites and garnet pyroxenites are easily within the P, T stability field of hydrous phlog (Konzett and Ulmer 1999; Fig. S6). Even so, a percolating potassic metasomatic melt will not precipitate phlogopite as long as phlogopite saturation is not reached. Partial reaction of a percolating melt is analogous to fractional crystallisation in that a residual melt develops that moves on and continues to transport K because its solidus temperature is lower than the ambient mantle temperature (Grassi and Schmidt 2011; Bulatov et al. 2014). With or without the metasomatic growth of phlog, metasomatism in eclogites is recognized by the introduction of incompatible trace elements into garnets and clinopyroxenes and is expressed by elevated LREE relative to HREE. Partial melting in the eclogite stability field results in increasingly steeper middle to heavy REE patterns and a drastic loss of LREE in the residue. Eclogites with positively sloping in middle to heavy REE patterns and elevated LREE should have therefore first partially melted and subsequently been metasomatized.

Modelling partial melting and metasomatism in the eclogite stability field – REE as tools

Modelling metasomatism requires the identification of a pre-metasomatic bulk rock, the definition of a metasomatic agent and a physical model of the metasomatic process. For magmatic precursor rocks the composition of a pre-metasomatic bulk rock may be the result of the composition of the primary melt, of fractional crystallisation processes, of high and low temperature alteration, of metamorphism and of partial melting. A further uncertainty arises from estimating of the mineral modes for bulk rock calculation. However, as has been shown in earlier studies (e.g. Jerde et al. 1993; Jacob 2004) and in this paper (electronic supplementary material Fig. S4) diagnostic features of trace elements remain for eclogites, even when the proportions of grt and cpx are varied within large limits.

Important information can also be extracted for major elements (Fig. 5). We can distinguish the Kimberley eclogites as Groups A (A-opx), B1 and B2 and deduce that the protoliths for A were higher pressure cumulates of mainly cpx with some ol and/or opx. We can also resolve that those for B1 had MORB-like compositions modified by partial melting. Focussing on sample KimPo 17 from Group A (Figs. 6a and 7a), we see that this reconstructed bulk rock composition has flat middle to heavy REE patterns and slightly depleted LREE. The shape is similar to N-MORB (Sun and McDonough 1989) but the abundances are 5 times lower. The other Group A samples have similar middle to heavy REE patterns but are severely enriched in LREE. This suggests that the metasomatic agent responsible for their enrichment had high LREE/HREE and was thus derived from a garnet-bearing source. Highly fractionated REE patterns also arise if we calculate the compositions of melts that were potentially in equilibrium with the LREE enriched Group A samples (electronic supplementary material Fig. S7). These theoretical melts are more fractionated than Group 2 kimberlites with drastically higher LREE abundances. Other chemical parameters like the prominent negative Ti, Zr-Hf and Nb-Ta anomalies may not represent the nature of the metasomatic agent because rutile was most likely present in all samples. Only the common presence of phlog reveals that the metasomatic agent was distinctly K-rich. We therefore used the composition of Group 2 kimberlites (Nowell et al. 2004) as the starting metasomatic agent composition for our modelling. The metasomatic process can be modelled as a percolation process or chromatographic fractionation during porous flow (e.g. Ionov et al. 2002) where the agent equilibrates with the substrate and a residual melt leaves the system. This melt from a first cell reacts with layers further up (second cell and so forth). The ensuing melt continuously change the composition on its way. For Group A we use sample KimPo 17 as the unmodified substrate because of its similarity to an unmodified cpx-rich cumulate and used Group 2 kimberlite for the first

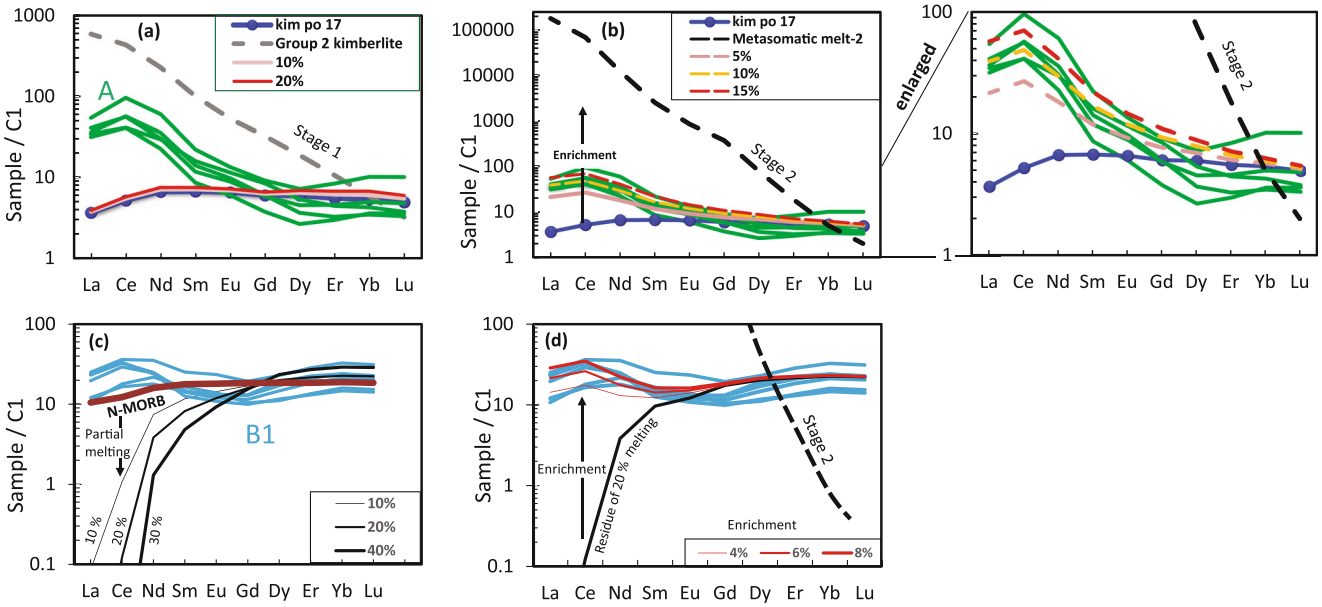

Fig. 7 **a** Modelled REE patterns calculated for various degrees of metasomatism using sample KimPo 17 as the substrate, Group 2 kimberlite from Nowell et al. (2004) as the metasomatic agent and the partition coefficients of Girnis et al. (2013). If 10 to 20% of the REE budget of a Group 2 kimberlite equilibrate with the substrate its REE contents are influenced only very little. This diagram, however, may mark stage 1 of a chromatographic fractionation process with residual melt moving on. **b** Using the same substrate but a more fractionated, residual melt derived from stage 1 the metasomatic overprint at stage-2 already overwhelms the LREE and generates patterns that overlap with those of Group A (% given in figure relative to REE of residual melt). **c** Model calculations for various degrees of fractional partial melting of Group B2 samples in the eclogite stability field. The starting composition is N-MORB from Sun and McDonough (1989), a grt:cpx ratio of 60:40 (vol%) was assumed for the bulk rock and 50:50 as the contribution to the melt. The partition coefficients are from Green et al. (2000). The fractionation of the middle and heavy REE of the natural samples are well mimicked by 20–40 vol% of partial melting. **d** Modelling of metasomatism Group B2 samples subsequent to partial melting using a calculated residue, a "stage-2" melt as in Fig. 7b as metasomatic agent and the partition coefficients of Girnis et al. (2013). The humped LREE patterns are well modelled by small degrees of metasomatism (< 10% of REE budget of the metasomatic agent)

reaction step and the partition coefficients from Girnis et al. (2013) to calculate modified REE patterns of the metasomatized rock and also the residual melt for various degrees of interaction. We find that the interaction with 10 and 20 vol% kimberlite does not change the REE patterns of the metasomatized rock very strongly (Fig. 7a). However, the effect on the composition of the residual melt is dramatic after interacting with rocks like eclogites with high amounts of garnet. Figure 7b shows the composition of the residual melt after equilibration in the first step. It is highly fractionated with LREE abundances of more than 10^5 times chondritic. Figure 7b (and its enlargement) also shows that 5 to 15 vol% of such a melt is sufficient to produce the range of REE compositions of Group A from a composition KimPo 17.

Group B1 eclogites shows enrichment in LREE with a hump at Ce, a trough at the MREE and positively sloped HREE (Figs. 6b and 7c–d). Such sinusoidal patterns are commonly reported from peridotitic samples (e.g. Stachel et al. 1998; Shu and Brey 2015). They require at least three stages in their development i) the generation of the protolith, ii) partial melting in the eclogite stability field and iii) subsequent metasomatism. The HREE concentrations of the lower abundance range of the Group B1 samples are close to N-MORB (Fig. 3a; Sun and McDonough 1989) but are fractionated to lower levels for the middle REE. As already explained above this is most likely due to partial melting. Batch melting model calculations for an N-MORB-like eclogite will increase fractionation of the middle to heavy REE (Fig. 7c). We then used the calculated residue for 20 vol% melting as the pre-metasomatic bulk rock, a metasomatic agent (residual melt) like that generated after the interaction of a kimberlitic melt in a first step and the partition coefficients of Girnis et al. (2013). Model calculation shows that the enriched, humped LREE patterns of the B1 samples can be generated by enrichment levels of 4 to 8 vol% (Fig. 7d).

Conclusions

Equilibration temperatures for a range of petrographically diverse Kimberley eclogite and garnet pyroxenite xenoliths show that they are derived from throughout the subcontinental lithospheric mantle, rather than being concentrated into a specific depth range. Petrographically and chemically distinct types of eclogites appear to come from discrete sections of the mantle root. Our expanded sample suite has

revealed significantly more complexity within these rocks than found previously. While our findings for the protoliths of the Group A agree with the oceanic cumulate origin proposed by Jacob et al. (2009) we suggest a basaltic or gabbroic origin for Group B1 eclogites. The anomalously high Na and Al and unusual REE patterns of the Group B-2 suite defined here make their protolith identification difficult and further work is needed to fully resolve this. The complex trace element signatures of the full spectrum of Kimberley eclogites belie a multi-stage history of melt depletion and metasomatism since their emplacement in the lithospheric mantle. Using constraints from other metasomatised Kimberly mantle rocks suggest that much of the metasomatic phlog in the eclogites formed during an intense episode of metasomatism that affected the mantle beneath this region 1.1 Gyr ago.

Acknowledgements The authors profited from the continuous help and support in the laboratory, in the field, and through discussions by Heidi E. Hoefer, Jan Heliosch, Vlad Matjuschkin, Yan Luo, Sarah Woodland, Chiranjeeb Sarkar and Jeffrey W. Harris. We particularly appreciate Jock Robey's help and support in making contact in the right places and in collecting the valuable specimens with us. Dr. Zhaochu Hu provided the opportunity and help for the trace element analysis of phlogopites at the State Key Laboratory of Geological Processes and Mineral Resources, China University of Geosciences (Wuhan). The valuable input of Sébastien Pilet and two anonymous reviewers, the guest editor David B. Snyder and the editor-in-chief Lutz Nasdala is highly appreciated. This research was supported by funding from the Canada Excellence Research Chairs program and by the Deutsche Forschungsgemeinschaft (BR1012/33-1).

References

Armstrong JT (1991) Quantitative elemental analysis of individual microparticles with electron beam instruments. In: Heinrich KFJ, Newbury DE (eds) Electron probe quantitation. Plenum Press, New York, London, pp 261–315

Armstrong JT (1995) CITZAF: a package of correction programs for the quantitative electron microbeam X-ray analysis of thick polished materials, thin films, and particles. Microb Anal 4:177–200

Aulbach S, Jacob DE (2016) Major- and trace-elements in cratonic mantle eclogites and pyroxenites reveal heterogeneous sources and metamorphic processing of low-pressure protoliths. Lithos 262: 586–605

Aulbach S, Viljoen KS (2015) Eclogite xenoliths from the Lace kimberlite, Kaapvaal craton: from convecting mantle source to palaeo-ocean floor and back. Earth Planet Sci Lett 431:274–286

Barth M, Rudnick RL, Horn I, McDonough WF, Spicuzza M, Valley JW, Haggerty SE (2001) Geochemistry of xenolithic eclogites from West Africa, part I: a link between low MgO eclogites and Archean crust formation. Geochim Cosmochim Acta 65:1499–1527

Basaltic Volcanism Study Project (1981) Basaltic volcanism on the Terrestrial planets. The Lunar and Planetary Institute, Houston. Pergamon Press, New York, 1286 pp

Bulatov VK, Brey GP, Girnis AV, Gerdes A, Höfer HE (2014) Carbonated sediment–peridotite interaction and melting at 7.5–12 GPa. Lithos 200-201:368–385

Casey JF (1997) Comparison of major and trace element geochemistry of abyssal peridotites and mafic plutonic rocks with basalts from the MARK region of the mid-Atlantic ridge. In: Karson JA, Cannat M, Miller DJ, Elthon D (eds) Proceedings of the ocean drilling program, scientific results. 153, pp 181–241

Coleman RG, Lrt DE, Bnamv LB, Bnalwocr WW (1965) Eclogites and eclogites; their differences and similarities. Geol Soc Am BulI 76: 83–508

Dawson JB, Smith JV (1977) MARID (mica-amphibole–rutile–ilmenite–diopside) suite of xenoliths in kimberlite. Geochim Cosmochim Acta 41(2):309–323

de Capitani C, Petrakakis K (2010) The computation of equilibrium assemblage diagrams with Theriak/Domino software. Am Mineral 95: 1006–1016

Dongrea AN, Jacob DE, Stern RA (2015) Subduction-related origin of eclogite xenoliths from Wajrakarur kimberlite field, Eastern Dharwar craton, Southern India: Constraints from petrology and geochemistry. Geochim Cosmochim Acta 166(1):165–188

Erlank AJ, Waters FG, Hawkesworth CJ, Haggerty SE, Allsopp HL, Rickard RS, Menzies MA (1987) Evidence for mantle metasomatism in peridotite nodules from the Kimberley pipes, South Africa. In: Menzies MA, Hawkesworth CJ (eds) Mantle Metasomatism. Academic Press, London, pp 221–311

Girnis A, Bulatov VK, Brey GP, Gerdes A, Höfer EH (2013) Trace element partitioning between mantle minerals and silicate–carbonate melts at 6-12 GPa and applications to mantle metasomatism and kimberlite genesis. Lithos 160-161:183–200

Grassi D, Schmidt MW (2011) Melting of carbonated pelites at 8–13 GPa: generating K-rich carbonatites for mantle metasomatism. Contrib Mineral Petrol 162:169–191

Green DH, Ringwood AE (1967) The genesis of basaltic magmas. Contrib Mineral Petrol 15:103–190

Green TH, Blundy JD, Adam J, Yaxley GM (2000) SIMS determination of trace element partition coefficients between garnet, clinopyroxene and hydrous basaltic liquids at 2–7.5 GPa and 1080–1200 °C. Lithos 53:165–187

Harte B, Kirkley MB (1997) Partitioning of trace elements between clinopyroxene and garnet: data from mantle eclogites. Chem Geol 136:1–24

Heaman LM, Creaser RA, Cookenboo HO, Chacko T (2006) Multi-stage modification of the Northern Slave mantle lithosphere: evidence from zircon- and diamond-bearing eclogite xenoliths entrained in Jericho kimberlite, Canada. J Petrol 47:821–858

Hellman PL, Henderson P (1977) Are rare earth elements mobile during spilitisation? Nature 267:38–40

Hopp J, Trieloff M, Brey GP, Woodland AB, Simon NSC, Wijbrans JR, Siebel W, Reitter E (2008) 40Ar/39Ar-ages of phlogopite in mantle xenoliths from South African kimberlites: evidence for metasomatic mantle impregnation during the Kibaran orogenic cycle. Lithos 106, 3-4:351–364

Ionov DA, Bodinier J-L, Mukasa SB, Zanetti A (2002) Mechanisms and sources of mantle metasomatism: major and trace element compositions of peridotite xenoliths from Spitsbergen in the context of numerical modelling. J Petrol 43(12):2219–2259

Jacob DE (2004) Nature and origin of eclogite xenoliths from kimberlites. Lithos 77:295–316

Jacob DE, Jagoutz E, Lowry D, Mattey D, Kudrjavtseva G (1994) Diamondiferous eclogites from Siberia: remnants of Archean oceanic crust. Geochim Cosmochim Acta 58:5191–5207

Jacob DE, Bizimis M, Salters VJM (2005) Lu/Hf and geochemical systematics of recycled ancient oceanic crust: evidence from Roberts Victor eclogites. Contrib Mineral Petrol 148(6):707–720

Jacob DE, Viljoen KS, Grassineau NV (2009) Eclogite xenoliths from Kimberley, South Africa -a case study of mantle metasomatism in eclogites. Lithos 112:1002–1013

Jenner FE, O'Neill HS (2012) Analysis of 60 elements in 616 ocean floor basaltic glasses. Geochem Geophys Geosyst 13(1):1–11

Jerde EA, Taylor LA, Crozaz G, Sobolev NV (1993) Exsolution of garnet within clinopyroxene of mantle eclogites: major- and trace-element chemistry. Contrib Mineral Petrol 114:148–159

Jochum KP, Willbold M, Raczek I, Stoll B, Herwig K (2005) Chemical characterisation of the USGS reference glasses GSA-1G, GSC-1G, GSD-1G, GSE-1G, BCR-2G, BHVO-2G and BIR-1G using EPMA, ID-TIMS, ID-ICPMS and LA-ICPMS. Geostand Geoanal Res 29:285–302

Klemme S, Blundy JD, Wood BJ (2002) Experimental constraints on major and trace element partitioning during partial melting of eclogite. Geochim Cosmochim Acta 66:3109–3123

Konzett J, Ulmer P (1999) The stability of hydrous potassic phases in lherzolitic mantle—an experimental study to 9·5 GPa in simplified and natural bulk compositions. J Petrol 4:629–652

Konzett J, Armstrong RA, Günther D (2000) Modal metasomatism in the Kaapvaal craton lithosphere: constraints on timing and genesis from U-Pb zircon dating of metasomatized peridotites and MARID-type xenoliths. Contrib Mineral Petrol 139:704–719

Krogh EJ (1988) The garnet-clinopyroxene Fe-Mg geothermometer - a reinterpretation of existing experimental data. Contrib Mineral Petrol 99:44–48

Lazarov M (2008) Archean to present day evolution of the lithospheric mantle beneath the Kaapvaal craton—processes recorded in subcalcic garnets, peridotites and polymict breccia. PhD thesis Goethe-University Frankfurt. http://publikationen.ub.uni-frankfurt.de/files/6873/LazarovMarina.pdf

Liu YS, Hu ZC, Gao S, Günther D, Xu J, Gao CG, Chen HH (2008) In situ analysis of major and trace elements of anhydrous minerals by LA-ICP-MS without applying an internal standard. Chem Geol 257(1–2):34–43

Liu YS, Gao S, Hu ZC, Gao CG, Zong KQ, Wang DB (2010) Continental and oceanic crust recycling-induced melt-peridotite interactions in the Trans-North China Orogen: U-Pb dating, Hf isotopes and trace elements in zircons of mantle xenoliths. J Petrol 51(1–2):537–571

Mather KA, Pearson DG, McKenzie D, Kjarsgaard B, Priestley K (2011) Constraining the depth and thermal history of cratonic lithosphere using peridotite xenolith and xenocryst thermobarometry and seismology. Lithos 125:729–742

Nowell GM, Pearson DG, Bell DR, Carlson RW, Smith CB, Kempton PD, Noble SR (2004) Hf isotope systematics of kimberlites and their megacrysts: new constraints on their source regions. J Petrol 45:1583–1612

Pearson DG (1999) The age of continental roots. Lithos 48:171–194

Perk NW, Coogan LA, Karson JA, Klein EM, Hanna HD (2007) Petrology and geochemistry of primitive lower oceanic crust from Pito Deep: implications for the accretion of the lower crust at the Southern East Pacific Rise. Contrib Mineral Petrol 154:575–590

Presnall DC, Dixon SA, Dixon JR, O'Donnel TH, Brenner NL, Schrock RL, Dycus DW (1978) Liquidus phase relations on the join Diopside-Forsterite-Anorthite from 1 atm to 20 kbar. Their bearing on the generation and crystallization of basaltic magma. Contrib Mineral Petrol 66:203–220

Purwin H, Lauterbach S, Brey GP, Woodland AB, Kleebe H-J (2012) An experimental study of the Fe oxidation states in garnet and clinopyroxene as a function of temperature in the system CaO–FeO–Fe_2O_3–MgO–Al_2O_3–SiO_2: implications for garnet–clinopyroxene geothermometry. Contrib Mineral Petrol 165:623–639

Ringwood AE (1975) Composition and petrology of the earth's mantle. Mac Graw Hill, New York

Schmickler B, Jacob DE, Foley SF (2004) Eclogite xenoliths from the Kuruman kimberlites, South Africa: geochemical fingerprinting of deep subduction and cumulate processes. Lithos 75(1–2):173–207

Schulze DJ (1989) Constraints on the abundance of eclogite in the upper mantle. J Geophys Res 94:4205–4212

Shu Q, Brey GP (2015) Ancient mantle metasomatism recorded in subcalcic garnet xenocrysts: temporal links between mantle metasomatism, diamond growth and crustal tectonomagmatism. Earth Planet Sci Lett 418:27–39

Shu Q, Brey GP, Hoefer HE, Zhao ZD, Pearson DG (2016) Kyanite/corundum eclogites from the Kaapvaal Craton: subducted troctolites and layered gabbros from the Mid to Early Archean. Contrib Mineral Petrol 171:1

Simon NSC, Carlson RW, Pearson DG, Davies G (2007) The origin and evolution of the Kaapvaal cratonic lithospheric mantle. J Petrol 48(3):589–625

Smyth JR, Hatton CJ (1977) Coesite-sanidine grospydite from Roberts-Victor kimberlite. Earth Planet Sci Lett 34:284–290

Sommer H, Jacob DE, Stern RA, Petts D, Mattey DP, Pearson DG (2017) Fluid-induced transition from banded kyanite- to bimineralic eclogite and implications for the evolution of cratons. Geochim Cosmochim Acta 207:19–42

Stachel T, Viljoen KS, Brey GP, Harris JW (1998) Metasomatic processes in lherzolitic and harzburgitic domains of diamondiferous lithospheric mantle: REE in garnets from xenoliths and inclusions in diamonds. Earth Planet Sci Lett 159:1–12

Sun S-S, McDonough WF (1989) Chemical and isotopic systematics of oceanic basalts: implications for mantle compositions and processes. In: Saunders AD, Norris MJ (eds) Magmatism in the ocean basins. Geol Soc Spec Publ, pp 313–345

Taylor LA, Neal CR (1989) Eclogites with oceanic crustal and mantle signatures from the Bellsbank kimberlite, South Africa, part 1: mineralogy, petrography, and whole rock chemistry. J Geol 97:551–567

Waters FG (1987) A suggested origin of MARID xenoliths in kimberlites by high pressure crystallization of an ultrapotassic rock such as lamproite. Contrib Mineral Petrol 95:523–533

Weiss Y, McNeill J, Pearson GD, Nowell GM, Ottley CJ (2015) Highly saline fluids from a subducting slab as the source for fluid-rich diamonds. Nature 524:339–344

Williams-Jones AE (2015) The hydrothermal mobility of the rare earth elements. British Columbia Geological Survey, Paper 2015-3:119–123